

New Constraints on Radii and Tidal Deformabilities of Neutron Stars from GW170817

Elias R. Most,¹ Lukas R. Weih,¹ Luciano Rezzolla,^{1,2} and Jürgen Schaffner-Bielich¹

¹*Institut für Theoretische Physik, Max-von-Laue-Straße 1, 60438 Frankfurt, Germany*

²*Frankfurt Institute for Advanced Studies, Ruth-Moufang-Straße 1, 60438 Frankfurt, Germany*



(Received 1 March 2018; revised manuscript received 15 May 2018; published 25 June 2018)

We explore in a parameterized manner a very large range of physically plausible equations of state (EOSs) for compact stars for matter that is either purely hadronic or that exhibits a phase transition. In particular, we produce two classes of EOSs with and without phase transitions, each containing one million EOSs. We then impose constraints on the maximum mass ($M < 2.16 M_{\odot}$) and on the dimensionless tidal deformability ($\tilde{\Lambda} < 800$) deduced from GW170817, together with recent suggestions of lower limits on $\tilde{\Lambda}$. Exploiting more than 10^9 equilibrium models for each class of EOSs, we produce distribution functions of all the stellar properties and determine, among other quantities, the radius that is statistically most probable for any value of the stellar mass. In this way, we deduce that the radius of a purely hadronic neutron star with a representative mass of $1.4 M_{\odot}$ is constrained to be $12.00 < R_{1.4}/\text{km} < 13.45$ at a 2σ confidence level, with a most likely value of $\bar{R}_{1.4} = 12.39$ km; similarly, the smallest dimensionless tidal deformability is $\tilde{\Lambda}_{1.4} > 375$, again at a 2σ level. On the other hand, because EOSs with a phase transition allow for very compact stars on the so-called “twin-star” branch, small radii are possible with such EOSs although not probable, i.e., $8.53 < R_{1.4}/\text{km} < 13.74$ and $\bar{R}_{1.4} = 13.06$ km at a 2σ level, with $\tilde{\Lambda}_{1.4} > 35.5$ at a 3σ level. Finally, since these EOSs exhibit upper limits on $\tilde{\Lambda}$, the detection of a binary with a total mass of $3.4 M_{\odot}$ and $\tilde{\Lambda}_{1.7} > 461$ can rule out twin-star solutions.

DOI: [10.1103/PhysRevLett.120.261103](https://doi.org/10.1103/PhysRevLett.120.261103)

Introduction.—On August 17, 2017, the Advanced LIGO and Virgo network of gravitational-wave detectors recorded the signal from the inspiral of a binary neutron-star system, i.e., event GW170817 [1]. Less than a couple of seconds later, the gravitational-wave signal was followed by a series of electromagnetic emissions. These electromagnetic counterparts have provided the long-sought confirmation that merging neutron-star binaries can be associated with short γ -ray bursts, shedding important light on the long-standing puzzle of the origin of these phenomena [2–5].

These multimessenger observations, together with numerical simulations of merging neutron stars (see [6,7] for recent reviews), and the modeling of the kilonova emission from this process [8–10] have provided important new insight on the maximum mass of neutron stars and on the expected distribution in radii [11–17]. The approaches followed in these works differ significantly in the techniques employed but provide a remarkably robust picture of what is the maximum mass of nonrotating stellar models M_{TOV} . For example, by combining the signal from GW170817 and quasiuniversal relations (see, e.g., [18,19]) that correlate M_{TOV} with the maximum mass supported through uniform rotation M_{max} [20] (see [21] for the case of differential rotation), Ref. [15] has set constraints on the maximum mass to be $2.01_{-0.04}^{+0.04} \leq M_{\text{TOV}}/M_{\odot} \lesssim 2.16_{-0.15}^{+0.17}$, where the lower limit comes from pulsar observations [22]. Similarly, by considering the most generic family of neutron-star-matter

equations of state (EOSs) that interpolate between recent nuclear-physics results at low and high baryon densities, Ref. [11] has set constraints for the radius of a $1.4 M_{\odot}$ neutron star to be $R_{1.4} < 13.6$ km, while the minimum dimensionless tidal deformability is $\tilde{\Lambda}_{1.4} > 120$.

In this Letter, we reconsider the problem of constraining the radii and tidal deformability of neutron stars considering more than two million different EOSs (with and without a phase transition) that are physically plausible and respect the observational constraints on the maximum mass. Using this large set of equilibria, we explore the distribution functions of stellar models and how they are affected by the imposition of various constraints, be they on the maximum mass or on the dimensionless tidal deformability.

Explorations of this type have been considered in the recent past, starting from the works of Refs. [23,24] (see also [25]), who derived limits on the neutron-star radius by using data from x-ray binaries combined with parameterized EOSs (see [26,27] for recent reviews). When compared with these approaches, our results benefit from several improvements. First, we impose, and in a differential manner, recent constraints on the maximum mass [13,15–17] and on the tidal deformability [10,14] coming directly from GW170817 and that obviously could not have been included by previous works, e.g., [23,24,28,29]. Second, we exploit recent improvements on the EOS of neutron matter in the outer core [30], which plays a fundamental role in determining the

stellar radius. Third, we carry out the first systematic study of the statistical properties of the tidal deformability highlighting that the lower limit for $\tilde{\Lambda}$ is very tightly constrained. Finally, we explore a more recent, but also more restricted, prescription for the outer core as infinite neutron matter [31] and compare to the results obtained using the setup employed by Ref. [11]. Hereafter, masses will be in units of solar masses and radii in kilometers.

Methods and setup.—We compute models of cold non-rotating neutron stars by numerically solving the Tolman-Oppenheimer-Volkoff (TOV) equations together with an EOS. As the complete EOS is unknown, we construct a parameterized set of EOSs by taking into account calculations that describe nuclear matter in the outer crust [32,33] and state-of-the-art descriptions of nuclear matter close to nuclear-saturation density [30,31], together with a perturbative QCD calculation for matter at densities exceeding that in the core of neutron stars [34,35]. Because the EOS at intermediate densities is not well known, we construct it using piecewise polytropes, overall following Ref. [36]. Additionally, we account for the existence of phase transitions by considering EOSs that admit a jump in the energy density between randomly chosen segments of the polytropes [29,37–39], thus allowing for “twin-star” solutions [40–42] (see Supplemental Material for details [43]).

Radius and tidal deformability constraints.—Figure 1 offers a complete view of the probability distribution functions (PDFs) built using our $\sim 2 \times 10^9$ stellar models.

The top-left panel, in particular, shows the color-coded PDF when only the *observational* constraints are imposed on the maximum mass [22] and on the tidal deformability [1], i.e., $2.01 < M_{\text{TOV}}$ and $\tilde{\Lambda}_{1.4} < 800$ (see Fig. 3 of Supplemental Material [43] for the PDF with only the maximum-mass constraint). Indicated with red solid and dashed lines are the values at which the corresponding cumulative distributions at a fixed mass reach a value of 2σ and 3σ , respectively, thus setting both a minimum and a maximum value for the radius at that mass with a probability of $\sim 95\%$ and 99.7% . Note that the PDF extends beyond the red lines but attains very small values in these regions. The top-right panel shows instead the PDF when, in addition to the lower limit, also an upper limit is set on the maximum mass, i.e., $2.01 < M_{\text{TOV}} < 2.16$ [15], while keeping the observational constraint on the tidal deformability. Note that the addition of this constraint changes the PDF, decreasing the average value of the maximum radius at a given mass. The bottom-left panel in Fig. 1 shows the impact of the combined observational and maximum mass constraints with that of a lower limit on the tidal deformability as suggested by Ref. [14], i.e., after considering $2.01 < M_{\text{TOV}} < 2.16$ and $400 < \tilde{\Lambda}_{1.4} < 800$. We note that, although the constraint $\tilde{\Lambda}_{1.4} > 400$ set by Ref. [14] does not come with a systematic quantification of the uncertainties, it is reasonable that such a lower limit exists on the basis of the considerations made by Ref. [14].

The effect of these combined constraints is to significantly reduce the variance in the small-radii region and to refine the

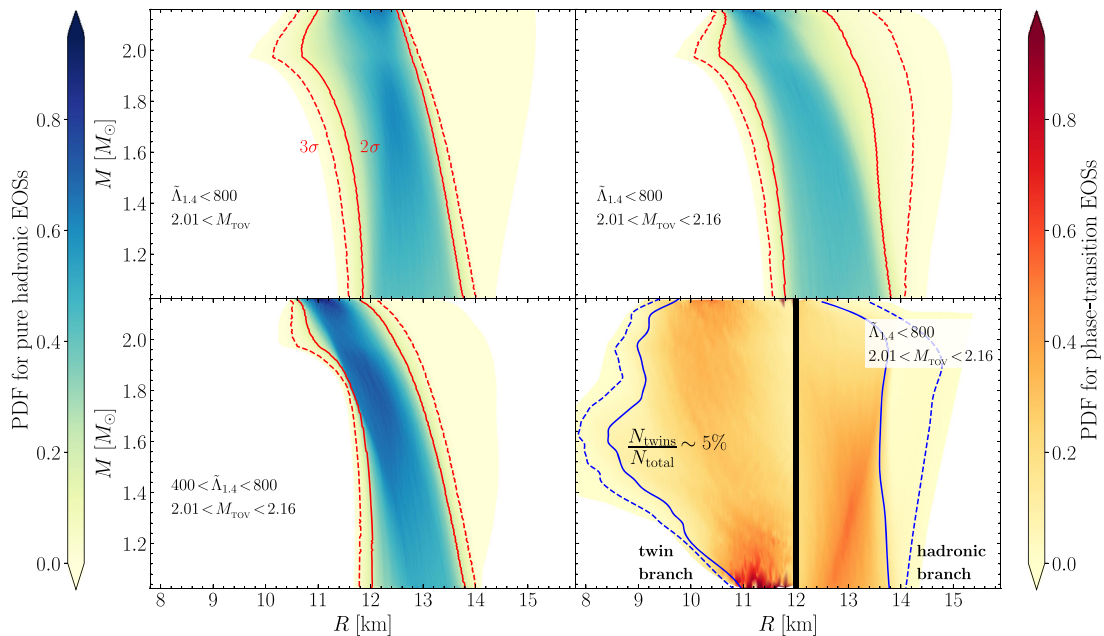


FIG. 1. PDFs of stellar radii. Top-left panel: PDF with only the observational constraints on the observed maximum mass and tidal deformability for pure hadronic EOSs; top right: PDF when also an upper limit is set on the maximum mass; bottom left: PDF with the combined constraints on maximum mass and tidal deformability; bottom right: the same as in the bottom left but for EOSs with a phase transition; the thick black line at 12 km distinguishes the PDFs of hadronic twin stars, which represent only 5% of the total sample with phase transitions. In all panels, the solid and dashed lines indicate the 2σ and 3σ confidence levels, respectively.

range for the most likely radii at a given mass. Note that the distribution now is not only restricted to a rather small range in radii, but it is also peaked around the small-radii end of the range. Because the EOS beyond nuclear-saturation density is not known, the possibility of phase transitions is also taken into account in the bottom-right panel, where we do not impose the $400 < \tilde{\Lambda}_{1.4}$ constraint, since it is based on a numerical simulation with EOSs without phase transitions. Furthermore, by splitting the panel at 12 km, we distinguish between the PDF of the hadronic branch and the PDF of the “twin-star” branch, namely, of all those stars that populate the small-radii second stable branch typical of models with a phase transition. Note that, while the PDF on the hadronic branch is very similar to the top-right panel, that of the twin-star branch is significantly different. In particular, we find that the radius varies in a much broader range, $8.53 < R_{1.4}/\text{km} < 13.74$, and is not as constrained as the hadronic branch; more importantly, the twin stars represent only $\sim 5\%$ of the total sample with phase transitions.

These last results are best appreciated when considering cuts of the bottom panels in Fig. 1 at a fixed value of the mass, e.g., 1.4. This is shown in the left panel in Fig. 2, which reports the PDF as a function of the radius at that mass, $R_{1.4}$. Shown with different lines are the distributions obtained when considering different constraints on the maximum mass or on the tidal deformability (see the legend). Note that when only the observational constraints are imposed, either on the maximum mass or on the tidal deformability, the distribution functions are rather broad and flat, with a width of about almost 3 km (cf. red and orange lines). On the other hand, when the combined constraints are considered, as shown with the green-shaded distribution, the variance decreases to about 2 km, and the PDF also exhibits a peak around the small-radii tail of the distribution. In this way, we are able to constrain $12.00 <$

$R_{1.4} < 13.45$ at a 2σ confidence level, with a most likely value of $\bar{R}_{1.4} = 12.45$. Although not shown in Fig. 2, we note that the PDFs are very robust upon changes in the upper limit of the maximum mass, when considering both smaller (2.1) or larger (2.33) values for M_{TOV} . Conversely, the PDFs are rather sensitive to changes in $\tilde{\Lambda}$. This is illustrated in the middle panel in Fig. 2, which shows how the reference green-shaded PDF varies when, for $M = 1.4$ and $2.01 < M_{\text{TOV}} < 2.16$, different intervals are considered for the tidal deformability (see the legend). Considering a large lower limit for the tidal deformability, e.g., from $\tilde{\Lambda}_{1.4} > 400$ to $\tilde{\Lambda}_{1.4} > 500$ (brown line), has the effect of excluding the softest EOSs and hence to shift the peak of the distribution to larger values, yielding a most likely value of $\bar{R}_{1.4} \simeq 13.0$ and a variance which is below 2 km. By contrast, changing the upper limit of the tidal deformability, e.g., taking the less conservative observational limit $\tilde{\Lambda}_{1.4} < 640$ [1] (orange line) or an even more conservative limit of $\tilde{\Lambda}_{1.4} < 1200$ (black line), does not change the distribution significantly.

Finally, when considering the distribution of models with phase transitions, the behavior in the right panel in Fig. 2 is rather different. While the application of the combined maximum mass and $\tilde{\Lambda}_{1.4}$ constraints yields the same results presented in the left panel (green- and orange-shaded curves), with $\bar{R}_{1.4} = 13.06$ at a 2σ level, the twin-star branch is much broader, i.e., $8.53 < R_{1.4} < 13.74$. Note that, although small-radii stars are possible, they are not probable and that the twin-branch stars are only $\sim 2\%$ of the total sample with a phase transition for $M = 1.4$. Also, note that if a constraint such as $\tilde{\Lambda}_{1.4} > 400$ could be applied to EOSs with phase transitions, it would only sharpen the mean value of the PDF for twin stars but again exclude the small-radii models of the hadronic branch (orange curve).

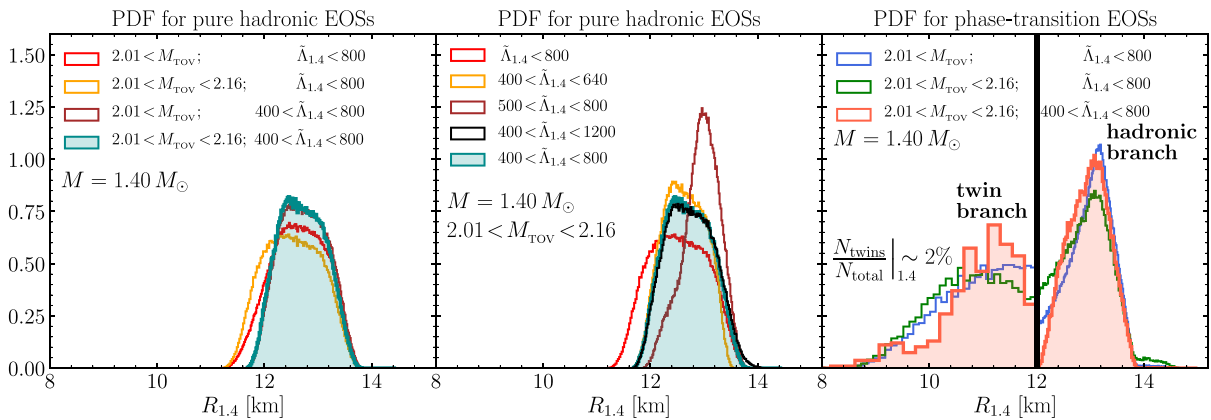


FIG. 2. PDFs of stellar radii for a neutron star with mass 1.4. Reported with different lines are the PDFs with different constraints on the maximum mass and tidal deformability (see the legends); the left and middle panels refer to pure hadronic EOSs, while the right one to EOSs with a phase transition (cf. Fig. 1).

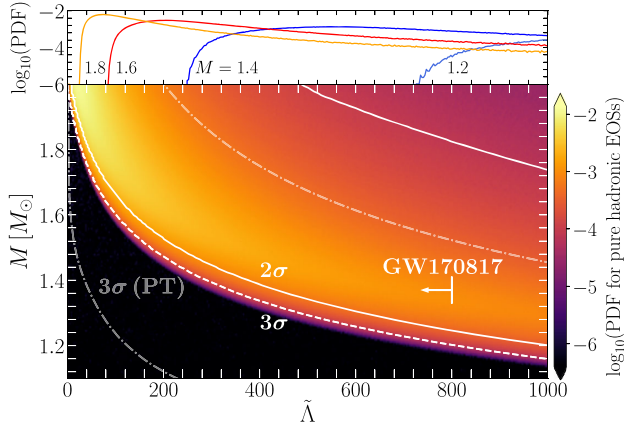


FIG. 3. PDF of the tidal deformability $\tilde{\Lambda}$ for pure hadronic EOSs satisfying the constraint $M_{\text{TOV}} > 2.01$. The white solid and dashed lines show where the corresponding cumulative distributions at a fixed mass reach a value of 2σ and 3σ , respectively. Also shown are the 3σ regions for an EOS featuring a phase transition. Shown with an arrow is the upper limit deduced from GW170817, while several cuts at fixed masses are shown in the top panel.

Additional information on the tidal deformability is presented in Fig. 3, which reports the PDF of $\tilde{\Lambda}$ for the hadronic EOS, with again the white solid (dashed) lines showing where the corresponding cumulative distributions at a fixed mass reach a value of 2σ (3σ). Furthermore, we indicate with gray dashed-dotted lines the 3σ values for EOSs with a phase transition (cf. Fig. 4 of Supplemental Material [43]). Shown instead with an arrow is the upper limit deduced from GW170817 [1]. The PDF in Fig. 3, which has not been presented before, points to three interesting properties. First, at any given mass, the PDF is highly asymmetrical and has a very sharp cutoff in the lower hand of the tidal deformability, which goes from $\tilde{\Lambda}_{\text{cutoff}} \sim 825$ at $M = 1.2$ to $\tilde{\Lambda}_{\text{cutoff}} \sim 285$ at $M = 1.4$ (see

the top panel in Fig. 3). Second, as the stellar mass increases, the distribution tends to a more pronounced peak and a smaller variance, with $0 \lesssim \tilde{\Lambda} \lesssim 480$ for $M = 2.0$. Finally, when considering a reference mass of 1.4, we can set $\tilde{\Lambda}_{1.4} > 375(290)$, again at a $2\sigma(3\sigma)$ confidence level, respectively. Similarly, the corresponding value for a 1.3(1.5) mass becomes $\tilde{\Lambda}_{1.3(1.5)} > 615(230)$ at 2σ . When allowing for phase transitions, we instead find that at $3\sigma \tilde{\Lambda}_{1.4} > 35.5$ and $\tilde{\Lambda}_{1.7} < 461$. Hence, a future gravitational-wave detection of a high-mass merger with a measured value of $\tilde{\Lambda}_{1.7} > 461$ can rule out twin stars below that mass. This is the first time that such upper limits have been provided on twin stars (see Supplemental Material [43] for an extended discussion).

As a concluding but important remark, we illustrate in Fig. 4 the impact that different treatments of the outer core may have on the statistical properties of neutron-star radii. In particular, the left panel in Fig. 4 shows the same distributions discussed in the bottom-left panel in Fig. 1 when following the treatment for the outer core discussed by Ref. [46], which is less conservative than the approach used here following Ref. [30]. Similarly, the right panel in Fig. 4 reports the corresponding distributions when the stellar models are built using improved neutron-matter calculations [31]. Leaving aside the details of the two different calculations, it is interesting that estimates for the outer core that are only slightly less conservative yield tighter constraints for $R_{1.4}$ and a PDF with a smaller variance (the light-shaded red lines refer to Ref. [30]); in particular, we obtain a variance of ~ 1 km at a 2σ level on the radii of low-mass stars. Figure 4 thus highlights that a more accurate knowledge of the matter in the outer core, i.e., for number densities in the range $0.08 \lesssim n/\text{fm}^{-3} \lesssim 0.21$, can have an enormous impact on the macroscopic properties of neutron stars. Any progress in this direction will impact our understanding of compact stars. For completeness, we comment that, while the

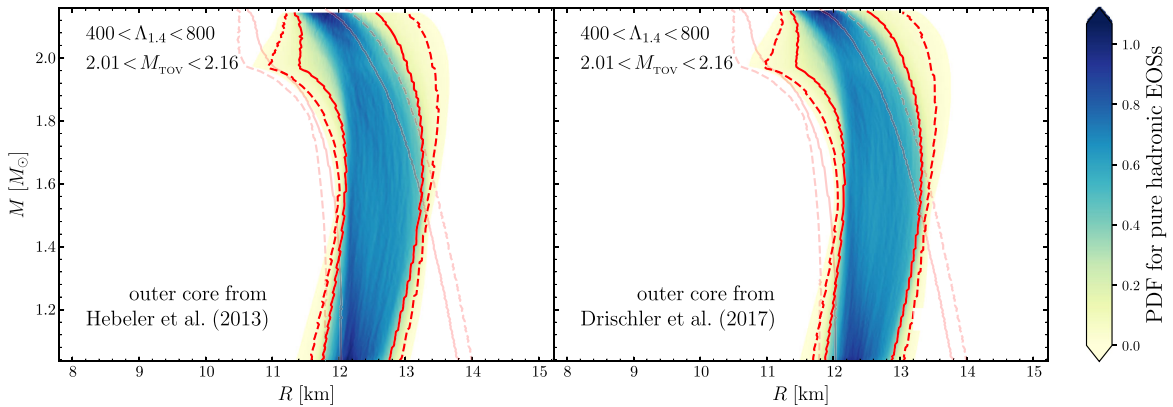


FIG. 4. Left panel: The same as in bottom-right panel in Fig. 1, but when the neutron matter in the outer core is treated following the approach of Ref. [46]. Right panel: The same as in the left panel but when considering the more recent prescription of Ref. [31] for the outer core. Shown as light shaded lines are the $2/3\sigma$ values reported in the bottom-right panel in Fig. 1.

results of Ref. [31] constrain the hadronic sector very well, we found their effect on the twin-star branch to be less pronounced.

Conclusions.—Using a parameterized construction of the EOS which matches realistic nuclear-physics calculations for the stellar crust at very low densities and perturbative QCD calculations at very high densities, we have constructed more than two million different EOSs, with and without phase transitions, that are physically plausible and compatible with the observations on the maximum mass. The corresponding PDFs have been studied to set constraints on the plausible values for the radii and tidal deformabilities of neutron stars. In particular, we have studied how the PDFs are affected by the imposition of new constraints on the maximum mass and on the tidal deformability that have been recently deduced via GW170817. These additional constraints induce significant changes in the PDFs, especially when they are imposed simultaneously. While the statistical properties of the stellar models vary only weakly with the maximum mass, constraints on the lower limit of the tidal deformability exclude the softest EOSs and shift the peak of the distribution to larger values, yielding a variance well below 2 km for purely hadronic EOSs, i.e., $12.00 < R_{1.4} < 13.45$ at a 2σ level, with a most likely value of $\bar{R}_{1.4} = 12.39$. On the other hand, the radii of twin stars are less constrained, namely, $8.53 < R_{1.4} < 13.74$, with very compact stars possible but not probable, so that $\bar{R}_{1.4} = 13.06$. We have also been able to set upper limits on the tidal deformability of hybrid stars, e.g., $\tilde{\Lambda}_{1.7} < 461$. For hadronic EOSs, an additional tightening of the uncertainties is achieved with refined descriptions of the outer core, thus calling for an improved characterization of the EOS at intermediate densities. Overall, our results show that GW170817 has had a profound impact on our ability to constrain the maximum mass, tidal deformability, and radii of neutron stars. New detections will provide even tighter constraints on the EOS of nuclear matter and restrict the radius of neutron stars to below the 10% uncertainty [47–50].

It is a pleasure to thank Christian Drischler, Arianna Carbone, Kai Hebeler, Jim Lattimer, Tyler Gorda, and Alekski Vuorinen for useful discussions. Support comes from “PHAROS,” COST Action CA16214; LOEWE-Program in Helmholtz International Centre (HIC) for FAIR; the DFG through Grant No. CRC-TR 211; and the European Union’s Horizon 2020 Research and Innovation Program (Grant No. 671698) (call FETHPC-1-2014, project ExaHyPE). E. R. M. and L. R. W. acknowledge support from Helmholtz Graduate School for Hadron and Ion Research (HGS-HIRE).

[1] B. P. Abbott *et al.* (LIGO Scientific Collaboration and Virgo Collaboration), *Phys. Rev. Lett.* **119**, 161101 (2017).

- [2] D. Eichler, M. Livio, T. Piran, and D. N. Schramm, *Nature (London)* **340**, 126 (1989).
- [3] R. Narayan, B. Paczynski, and T. Piran, *Astrophys. J. Lett.* **395**, L83 (1992).
- [4] L. Rezzolla, B. Giacomazzo, L. Baiotti, J. Granot, C. Kouveliotou, and M. A. Aloy, *Astrophys. J. Lett.* **732**, L6 (2011).
- [5] E. Berger, *Annu. Rev. Astron. Astrophys.* **52**, 43 (2014).
- [6] L. Baiotti and L. Rezzolla, *Rep. Prog. Phys.* **80**, 096901 (2017).
- [7] V. Paschalidis, *Classical Quantum Gravity* **34**, 084002 (2017).
- [8] L. Bovard, D. Martin, F. Guercilena, A. Arcones, L. Rezzolla, and O. Korobkin, *Phys. Rev. D* **96**, 124005 (2017).
- [9] B. D. Metzger, *Living Rev. Relativity* **20**, 3 (2017).
- [10] A. Perego, D. Radice, and S. Bernuzzi, *Astrophys. J. Lett.* **850**, L37 (2017).
- [11] E. Annala, T. Gorda, A. Kurkela, and A. Vuorinen, *Phys. Rev. Lett.* **120**, 172703 (2018).
- [12] A. Bauswein, O. Just, H.-T. Janka, and N. Stergioulas, *Astrophys. J. Lett.* **850**, L34 (2017).
- [13] B. Margalit and B. D. Metzger, *Astrophys. J. Lett.* **850**, L19 (2017).
- [14] D. Radice, A. Perego, F. Zappa, and S. Bernuzzi, *Astrophys. J. Lett.* **852**, L29 (2018).
- [15] L. Rezzolla, E. R. Most, and L. R. Weih, *Astrophys. J. Lett.* **852**, L25 (2018).
- [16] M. Ruiz, S. L. Shapiro, and A. Tsokaros, *Phys. Rev. D* **97**, 021501 (2018).
- [17] M. Shibata, S. Fujibayashi, K. Hotokezaka, K. Kiuchi, K. Kyutoku, Y. Sekiguchi, and M. Tanaka, *Phys. Rev. D* **96**, 123012 (2017).
- [18] K. Yagi and N. Yunes, *Phys. Rep.* **681**, 1 (2017).
- [19] B. Haskell, R. Ciolfi, F. Pannarale, and L. Rezzolla, *Mon. Not. R. Astron. Soc. Lett.* **438**, L71 (2014).
- [20] C. Breu and L. Rezzolla, *Mon. Not. R. Astron. Soc.* **459**, 646 (2016).
- [21] L. R. Weih, E. R. Most, and L. Rezzolla, *Mon. Not. R. Astron. Soc.* **473**, L126 (2018).
- [22] J. Antoniadis *et al.*, *Science* **340**, 1233232 (2013).
- [23] F. Özel, G. Baym, and T. Güver, *Phys. Rev. D* **82**, 101301 (2010).
- [24] A. W. Steiner, J. M. Lattimer, and E. F. Brown, *Astrophys. J.* **722**, 33 (2010).
- [25] F. Özel and D. Psaltis, *Phys. Rev. D* **80**, 103003 (2009).
- [26] J. M. Lattimer and M. Prakash, *Phys. Rep.* **621**, 127 (2016).
- [27] F. Özel and P. Freire, *Annu. Rev. Astron. Astrophys.* **54**, 401 (2016).
- [28] G. Hagen *et al.*, *Nat. Phys.* **12**, 186 (2016).
- [29] A. W. Steiner, C. O. Heinke, S. Bogdanov, C. Li, W. C. G. Ho, A. Bahramian, and S. Han, *Mon. Not. R. Astron. Soc.* **476**, 421 (2018).
- [30] C. Drischler, A. Carbone, K. Hebeler, and A. Schwenk, *Phys. Rev. C* **94**, 054307 (2016).
- [31] C. Drischler, K. Hebeler, and A. Schwenk, arXiv: 1710.08220.
- [32] G. Baym, C. Pethick, and P. Sutherland, *Astrophys. J.* **170**, 299 (1971).

- [33] J. W. Negele and D. Vautherin, *Nucl. Phys.* **A207**, 298 (1973).
- [34] A. Kurkela, P. Romatschke, and A. Vuorinen, *Phys. Rev. D* **81**, 105021 (2010).
- [35] E. S. Fraga, A. Kurkela, and A. Vuorinen, *Astrophys. J. Lett.* **781**, L25 (2014).
- [36] A. Kurkela, E. S. Fraga, J. Schaffner-Bielich, and A. Vuorinen, *Astrophys. J.* **789**, 127 (2014).
- [37] J. M. Lattimer and A. W. Steiner, *Astrophys. J.* **784**, 123 (2014).
- [38] I. Tews, J. Carlson, S. Gandolfi, and S. Reddy, *arXiv*:1801.01923.
- [39] I. Tews, J. Margueron, and S. Reddy, *arXiv*:1804.02783.
- [40] M. G. Alford, S. Han, and M. Prakash, *Phys. Rev. D* **88**, 083013 (2013).
- [41] D. E. Alvarez-Castillo and D. B. Blaschke, *Phys. Rev. C* **96**, 045809 (2017).
- [42] J.-E. Christian, A. Zacchi, and J. Schaffner-Bielich, *Eur. Phys. J. A* **54**, 28 (2018).
- [43] See Supplemental Material at <http://link.aps.org/supplemental/10.1103/PhysRevLett.120.261103> for details on the EOS and the impact of phase transitions, which includes Refs. [44, 45].
- [44] K. Hebeler, S. K. Bogner, R. J. Furnstahl, A. Nogga, and A. Schwenk, *Phys. Rev. C* **83**, 031301 (2011).
- [45] S. De, D. Finstad, J. M. Lattimer, D. A. Brown, E. Berger, and C. M. Biwer, *arXiv*:1804.08583.
- [46] K. Hebeler, J. M. Lattimer, C. J. Pethick, and A. Schwenk, *Astrophys. J.* **773**, 11 (2013).
- [47] L. Rezzolla and K. Takami, *Phys. Rev. D* **93**, 124051 (2016).
- [48] S. Bose, K. Chakravarti, L. Rezzolla, B. S. Sathyaprakash, and K. Takami, *Phys. Rev. Lett.* **120**, 031102 (2018).
- [49] K. Chatziioannou, J. A. Clark, A. Bauswein, M. Millhouse, T. B. Littenberg, and N. Cornish, *Phys. Rev. D* **96**, 124035 (2017).
- [50] H. Yang, V. Paschalidis, K. Yagi, L. Lehner, F. Pretorius, and N. Yunes, *Phys. Rev. D* **97**, 024049 (2018).